Monthly Notices
of the
ROYAL ASTRONOMICAL SOCIETY

Mon. Not. R. Astron. Soc. (2012) doi:10.1111/j.1365-2966.2012.20950.x

The role of the ergosphere in the Blandford–Znajek process

Milton Ruiz,[1⋆] Carlos Palenzuela,[2⋆] Filippo Galeazzi[3⋆] and Carles Bona[4⋆]

[1]*Departament de Física, Universitat de les Illes Balears, Crta. Valldemossa km 7.5, E-07122 Palma, Spain*
[2]*Canadian Institute for Theoretical Astrophysics, Toronto, Ontario M5S 3H8, Canada*
[3]*Max-Planck-Institut für Gravitationsphysik, Albert-Einstein-Institut, D-14476 Potsdam-Golm, Germany*
[4]*Departamento de Astronomía y Astrofísica, Universitat de València, 46100 Burjassot (Valencia), Spain*

Accepted 2012 March 19. Received 2012 March 14

ABSTRACT

The Blandford–Znajek process, one of the most promising models for powering relativistic jets from black holes, was initially introduced as a mechanism in which the magnetic fields extract energy from a rotating black hole. We study the evolution of force-free electromagnetic fields, which are generated by rapidly rotating stars, on regular space–times with an ergosphere. Our conclusive results confirm previous works, claiming that the Blandford–Znajek mechanism is not directly related to the horizon of the black hole. We also show that the radiated energy depends exponentially on the compactness of the star.

Key words: gravitation – magnetic fields – relativistic processes – methods: numerical.

1 INTRODUCTION

The Blandford–Znajek (BZ) process is one of the leading models to explain the launching of powerful relativistic jets emerging from the supermassive black holes at the centres of galaxies (i.e. active galactic nuclei), and the more moderate ones coming from stellar mass black holes (i.e. microquasars). The main ingredients of this process are a central rotating black hole and an accretion disc, which supports a magnetic field threading the black hole horizon. This magnetic field is twisted by the spinning black hole, producing an outgoing electromagnetic flux which extracts energy and angular momentum from the space–time.

Although the BZ model was introduced a long time ago (Blandford & Znajek 1977), it is only recently that many issues and theoretical discoveries concerning this mechanism have been settled. These advances on the understanding of the BZ process have been enabled by numerical simulations. For instance, it has been shown that only the magnetic field lines threading the ergosphere of the black hole (i.e. the region near the black hole where negative Killing energies can exist) rotate due to the frame dragging effect, whether or not they cross the horizon (Komissarov 2002, 2004, 2005, 2009). These twisted magnetic fields carry the energy of the relativistic jet, which seems to come from the ergosphere. Moreover, it is now understood how the luminosity depends on the black hole spin magnitude (Tchekhovskoy, Narayan & McKinney 2010; Palenzuela et al. 2010a) and its orientation (Palenzuela et al. 2010a). Moreover, the robustness of the process with respect to different boundary conditions (Palenzuela et al. 2011) and its resemblance to ideal magnetohydrodynamics (MHD) solutions in the limit of high magnetization (McKinney & Gammie 2004; Komissarov 2005) have also been shown. A generalization of the BZ process to boosted non-spinning black holes has also been investigated by Neilsen et al. (2011), where the magnetic fields extract the translational kinetic energy from the black holes. In this case, there is also an extraction of rotational energy through the original BZ process if the boosted black holes are also spinning. During the coalescence of a binary black hole surrounded by a magnetized circumbinary disc, this generalized BZ process will produce a dual jet structure during the inspiral phase which will result in a single BZ jet after the merger (Palenzuela, Lehner & Liebling 2010b).

The basic effects of the BZ mechanism can be explained by invoking the membrane paradigm (see Thorne & Macdonald 1982; Thorne et al. 1986 for details), which endows the black hole horizon with some physical properties like a surface charge density and resistivity. The problem is then reduced to a spherical conductor with a relative motion with respect to asymptotic magnetic field lines via rotation or translation. The magnetic field is produced by an external source and described by the force-free approximation. In spite of its simplicity and relative success, this analogy does not yet explain the source of the energy, which cannot be assigned to the horizon due to causality arguments (Punsly & Coroniti 1989, 1990). The membrane paradigm implies that the key ingredient of the mechanism is the black hole horizon, in contrast with the arguments, pointing rather to the ergosphere, presented by Komissarov. Because of the intrinsic marriage of the horizon and the ergosphere on black hole space–times, one could confuse the physical phenomena generated by each of them. It is therefore desirable to study the effect of each component separately.

In this paper, we perform a systematic study of the isolated effect of the ergosphere in the electromagnetic (EM) fields, by considering regular space–times produced by rapidly rotating neutron stars. By increasing the compactness of the star, an ergosphere

⋆E-mail: milton.ruiz@uib.es (MR); palen@cita.utoronto.ca (CP); filga@aei.mpg.de (FG); cbona@uib.es (CB)

appears with a toroidal topology (see Ansorg, Kleinwachter & Meinel 2002 for details). The compact object is immersed in a force-free environment produced by an externally sourced magnetic field. We will assume that the force-free EM fields are not coupled to the fluid, so their dynamics will be determined only by their evolution equations and by the properties of the curved space–time. Our aim is to analyse the precise role of the ergosphere on the activation of the BZ mechanism.

This paper is organized as follows. A detailed description of our model and a summary of the force-free evolution equations on a curved background are presented in Section 2. Some known results for stationary and axisymmetric space–times are summarized in Section 3. The numerical set-up and the initial data are described in Section 4, while our numerical results are discussed in Section 5. Finally, we summarize our results and conclude in Section 6. The robustness of our solutions against several sources of error is studied in Appendix A.

2 MODEL OF PASSIVE FORCE-FREE ENVIRONMENT

We consider the evolution of a magnetized plasma with negligible inertia on the space–time produced by a rotating compact star which is assumed to be both stationary and axisymmetric. Our approach will involve the resolution of two different systems of equations. On the one hand, the initial data are obtained by solving the Einstein equations coupled to the hydrodynamic equations. We will use an initial data solver developed by Ansorg et al. (2002) in order to obtain the solution for both the fluid and the space–time geometry. On the other hand, we will evolve the hyperbolic partial differential equation (PDE) system for the low-inertia magnetized plasma on this curved background, which can be described by the force-free approximation of the Maxwell equations. An important point of our model is that it neglects any coupling between the plasma and the fluid of the star. In this way, the EM fields will not interact directly with the fluid, and its evolution will be determined solely by the force-free equations in a curved space–time. In this section, we summarize the formulation used to describe these systems of equations. In particular, we review in detail the Eulerian description of electrodynamics in the force-free approximation.

2.1 The 3+1 decomposition

We consider a space–time (M, g_{ab}) which is foliated by a family of space-like hypersurfaces Σ_t parametrized by time function t. The induced metric on these spatial hypersurfaces is denoted by γ_{ij}. Coordinates defined on adjacent hypersurfaces can be related through the lapse function α, which measures the proper time elapsed between both hypersurfaces, and the shift vector β^i, which controls how the spatial coordinates propagate from one hypersurface to the next. An observer moving along the normal direction to the hypersurfaces (Eulerian observer) will have a coordinate speed given by $-\beta^i$, and will measure a proper time $\mathrm{d}\tau = \alpha\,\mathrm{d}t$. In terms of these quantities, it is possible to bring the metric of the space–time into the form

$$\begin{aligned} \mathrm{d}s^2 &= g_{ab}\,\mathrm{d}x^a\,\mathrm{d}x^b \\ &= -\alpha^2\,\mathrm{d}t^2 + \gamma_{ij}(\mathrm{d}x^i + \beta^i\mathrm{d}t)\,(\mathrm{d}x^j + \beta^j\mathrm{d}t). \end{aligned} \tag{1}$$

Here, and in what follows, Latin indices from the beginning of the alphabet (a, b, c, ...) denote four-dimensional space–time quantities, whereas Latin indices from the middle of the alphabet (i, j, k, ...) are spatial. It is also convenient to introduce the extrinsic curvature K_{ij}, which is associated with the way in which the hypersurfaces are immersed in the space–time (M, g_{ab}), in the form

$$K_{ij} = -\frac{1}{2\alpha}(\partial_t - \mathcal{L}_\beta)\,\gamma_{ij}. \tag{2}$$

Note that the Eulerian observer is defined independent of the space coordinates. It can be interpreted as being at rest in the hypersurface Σ_t. In the context of spinning stars or black holes, this observer is also called the locally non-rotating observer or zero-angular-momentum observer (ZAMO).

2.2 3+1 decomposition of the Maxwell equations

The covariant Maxwell equations are given by

$$\nabla_b F^{ab} = 4\pi I^a, \qquad \nabla_b {}^*F^{ab} = 0, \tag{3}$$

where I^b is the 4-current and F^{ab}, ${}^*F^{ab}$ are the Maxwell and the Faraday tensors, respectively. In order to provide an Eulerian description of the above equations, it is convenient to introduce the electric and magnetic fields measured by those observers, namely

$$E^a = F^{ab} n_b, \qquad B^a = {}^*F^{ab} n_b, \tag{4}$$

where n^a is the unit vector normal to the hypersurface Σ_t. Note that if the electric and magnetic susceptibilities of the medium vanish, as in vacuum or in a highly ionized plasma, the Faraday tensor becomes the dual of the Maxwell tensor. In a similar way, we define the charge density and current as

$$q = -I^a\, n_a, \qquad J^a = \perp^a_b\, I^b, \tag{5}$$

where $\perp^a_b = \delta^a{}_b + n^a\, n_b$ is the projection operator on to the hypersurface Σ_t. Using the previous definitions, the Maxwell equations can be rewritten as

$$(\partial_t - \mathcal{L}_\beta)E^i = \epsilon^{ijk} D_j(\alpha B_k) + \alpha K E^i - 4\pi\alpha\, J^i, \tag{6}$$

$$(\partial_t - \mathcal{L}_\beta)B^i = -\epsilon^{ijk} D_j(\alpha E_k) + \alpha\, K B^i, \tag{7}$$

$$D_i E^i = 4\pi q, \qquad D_i B^i = 0. \tag{8}$$

Here, $D_i = \perp^a_i \nabla_a$ is the covariant derivative associated with the spatial metric γ_{ij} and ϵ^{ijk} is the Levi–Civita tensor.

It is useful to introduce, for later convenience, the vector potential $\mathcal{U}_a$ which can be decomposed into

$$\Phi = -\mathcal{U}_a\, n^a, \qquad A_a = \perp^b_a\, \mathcal{U}_b. \tag{9}$$

In terms of this vector potential, the Maxwell tensor can be written down as

$$F_{ab} = -2\nabla_{[a}\mathcal{U}_{b]}. \tag{10}$$

On the other hand, the electromagnetic energy–momentum tensor,

$$T_{ab} = \frac{1}{4\pi}\left[F_a{}^c F_{bc} - \frac{1}{2}\, g_{ab}\, F^{cd} F_{cd}\right], \tag{11}$$

can be decomposed in the form

$$T_{ab} = \mathcal{E} n_a\, n_b + 2 n_{(a}\, S_{b)} + S_{ab}, \tag{12}$$

where $\mathcal{E}$, S_a and S_{ab} correspond to the local electromagnetic energy density, the momentum density (Poynting vector) and the spatial stress tensor as measured by the Eulerian observer. Finally, the local conservation of the energy–momentum tensor (11) is given by

$$\nabla_b T^{ab} = -F^{ab} I_b. \tag{13}$$

The key point about this discussion is that it has been formulated in terms of physical quantities measured by the Eulerian observer (ZAMO). In order to close the system of the Maxwell equations, where a relation between the EM fields and the electric current is required, one can use quantities measured by the Eulerian observer in the same way as in the special relativistic electrodynamics (see MacDonald & Thorne 1982; Komissarov 2004 for details).

2.3 Force-free approximation

The force-free approximation is valid in magnetized plasmas when the electromagnetic energy density $\mathcal{E}$ dominates over the matter energy density. It happens, for instance, in the magnetospheres of neutron stars or black holes, where the density of the plasma is so extremely low that even moderate magnetic field stresses will dominate over the fluid pressure gradients. In this limit, the stress–energy tensor of the plasma therefore satisfies

$$T^{ab} = T^{ab}_{\rm fluid} + T^{ab}_{\rm EM} \simeq T^{ab}_{\rm EM}. \tag{14}$$

The local conservation of this stress–energy tensor implies that the Lorentz force vanishes, $F^{ab}\, I_b \simeq 0$ (Goldreich & Julian 1969; Blandford & Znajek 1977). This expression can be written, in terms of 3+1 quantities, as

$$E^l\, J_l = 0, \qquad q\, E^l + \epsilon^{ljk}\, J_j\, B_k = 0. \tag{15}$$

Taking the scalar and the vector product between the magnetic field B^i and the spatial projection of the Lorentz force (15), we obtain

$$E^l B_l = 0, \qquad J^i = \frac{1}{B^2}\left(J^i_{\parallel} + J^i_{\perp}\right), \tag{16}$$

where $J^i_{\parallel}$ and $J^i_{\perp}$ are the components of the current parallel and perpendicular to the magnetic field B^i, respectively. These are defined as

$$J^i_{\parallel} = J^l\, B_l\, B^i, \qquad J^i_{\perp} = q\, \epsilon^{ijk}\, E_j\, B_k. \tag{17}$$

The first relation in equation (16) implies that the electric and magnetic fields must be perpendicular. The second relation defines the current up to the parallel component $J_{\parallel}$. Using the Maxwell equations, one can compute $(\partial_t - \mathcal{L}_\beta)(E^l\, B_l) = 0$, which has to vanish due to equation (15). This condition imposes a constraint for $J_{\parallel}$, which can be substituted into equation (16) to complete the specification of the current (see Gruzinov 2007 for details). We will use instead an alternative prescription to enforce the force-free conditions, which has been used successfully in previous studies of force-free magnetospheres (Spitkovsky 2006; Palenzuela et al. 2010a).

3 STATIONARY AND AXISYMMETRIC SPACE–TIMES

In the previous section, we have summarized the Maxwell equations and the force-free approximation on a generic space–time. Nevertheless, since we are interested in stationary and axisymmetric space–times, one can consider a set of coordinates adapted to these symmetries. In these coordinates, the metric of the space–time can be brought into the standard form (Lewis 1932; Papapetrou 1966)

$$\mathrm{d}s^2 = -\alpha^2\, \mathrm{d}t^2 + g_{\phi\phi}\,(\mathrm{d}\phi - \omega\, \mathrm{d}t)^2 + g_{rr}\, \mathrm{d}r^2 + g_{\theta\theta}\, \mathrm{d}\theta^2, \tag{18}$$

where the metric coefficients $\{\alpha, \omega, g_{rr}, g_{\theta\theta}, g_{\phi\phi}\}$ depend only on r and θ. Note that this metric describes usual astrophysical objects such as neutron star or black hole space–times. In particular, the Kerr metric can be written in the above form (Bergamini & Viaggiu 2004). As mentioned earlier, the shift vector is related to the relative velocity between the Eulerian observer and the stationary spatial coordinates. One can then interpret ω as the drag velocity of this observer with respect to the hypersurface Σ_t.

Using the decomposition of the Maxwell tensor in terms of the vector potential (9), the condition of axisymmetry and stationarity implies that the electric field is purely poloidal, $E_\phi = 0$. According to equation (16), it follows that E^i is perpendicular to the poloidal components of the magnetic field, so that one can rewrite E^i in the form

$$E^i = \epsilon^i{}_{jk}\, B^j\, U^k, \tag{19}$$

where U^k is an axial vector given by (Komissarov 2004)

$$U^a = \frac{1}{\alpha}\,(\Omega - \omega)\chi^a, \tag{20}$$

and $\chi^a = \partial_\phi$ is the axial Killing vector of the space–time. Note that according to equation (18), the shift vector is $\beta^k = -\omega\, \chi^k$. Therefore, one can interpret the velocity U^i as the velocity of the magnetic field relative to the Eulerian observer and Ω as the angular velocity of the magnetic lines, which can be written in terms of the Maxwell tensor as (Blandford & Znajek 1977)

$$\Omega = \frac{F_{tr}}{F_{t\phi}} = \frac{F_{t\theta}}{F_{\theta\phi}}. \tag{21}$$

It is also useful to calculate the scalar $B^2 - E^2$ which, using the electric field defined by equation (19), takes the form

$$(B^2 - E^2)\,\alpha^2 = B^2\alpha^2 - g_{\phi\phi} B_p^2\,(\Omega - \omega)^2, \tag{22}$$

where $B_p^2 = B_r\, B^r + B_\theta\, B^\theta$ is the magnitude of the poloidal component of the magnetic field. This relation implies a change of the sign of this invariant in highly compact rotating space–times with large $g_{\phi\phi}/\alpha^2$ and ω. Note that in electrovacuum scenarios, the Maxwell equations imply that B^ϕ vanishes. In this case, one can also assume that the magnetic field is generated by the distant plasma of large inertia, which means that the resulting magnetosphere will reach a steady state when $\Omega = 0$. This implies that the invariant (22) becomes

$$(B^2 - E^2)\,\alpha^2 = B_p^2\,(\alpha^2 - \beta^2). \tag{23}$$

Inside the ergosphere $\alpha^2 - \beta^2 < 0$. Therefore, the change of the sign of the invariant is related, at least in electrovacuum, with the presence of an ergosphere.

Finally, it is possible to define conserved quantities associated with the Killing vectors of the space–time $\xi^a = \partial_t$ and $\chi^a = \partial_\phi$. On the one hand, the redshifted energy density, corresponding to the Killing vector ξ^a, is defined as (see Blandford & Znajek 1977; MacDonald & Thorne 1982)

$$\mathcal{E}_\xi = T^{ab}\, \xi_a\, n_b = \alpha\, \mathcal{E} + \omega\, S^i\, \chi_i, \tag{24}$$

with the flux of energy given by

$$S^i_\xi = -T^{bc}\, \perp^i{}_b\, \xi_c = \alpha\, S^i + \omega\, S^{ij}\, \chi_j. \tag{25}$$

On the other hand, the angular momentum density, associated with the Killing vector χ^i, is defined

$$\mathcal{E}_\chi = -T^{ab}\, \chi_a\, n_b = S^i\, \chi_i, \tag{26}$$

with a flux of angular momentum given by

$$S^i_\chi = T^{bc}\, \perp^i{}_b\, \chi_c = S^{ij}\, \chi_j. \tag{27}$$

Since E_ϕ vanishes, the poloidal flux vector S^i_χ satisfies

$$S^p_\chi = -\frac{1}{4\pi}\,(B^l\,\chi_l)\,B^p. \tag{28}$$

Using this condition and equation (16), it is straightforward to show that

$$S^p_\xi = \Omega\,S^p_\chi. \tag{29}$$

Therefore, both the flux of the redshifted energy and the flux of angular momentum are transported along the poloidal field lines.

According to equation (25), the EM-radiated energy crossing a spherical surface at a given radius is

$$\partial_t S = 2\pi \int_0^\pi \sqrt{-g}\,S^r_\xi\,\mathrm{d}\theta. \tag{30}$$

Note that on a regular space–time in Lewis–Papapetrou coordinates (18), the radiated energy flux density S^r_ξ is given by

$$S^r_\xi = -\frac{\Omega}{2\pi}\,B^r B^\phi \alpha^2 g_{\phi\phi}. \tag{31}$$

Moreover, in the case of a Kerr space–time in Lewis–Papapetrou coordinates (Bergamini & Viaggiu 2004), the above expression becomes

$$S^r_\xi = -\frac{\Omega}{2\pi}\,B^r B^\phi \Delta, \tag{32}$$

where $\Delta = r^2 + a^2 - 2Mr$. Since the Kerr space–time in these coordinates is singular at the horizon, it is convenient to transform to other coordinates that penetrate the horizon smoothly. This is the case for the Kerr–Schild coordinates, where the energy flux density S^r_ξ can be written as

$$S^r_\xi = \frac{\Omega\, r}{2\pi}\,(B^r)^2\,\left(\frac{a}{2\,M\,r} - \Omega\right)\,\sin^2\theta - \frac{\Omega}{4\pi}\,\Delta\,B^r\,B^\phi\,\sin^2\theta. \tag{33}$$

At the horizon, where $r = r_\mathrm{H}$ and $\Delta = 0$, it becomes

$$S^r_\xi|_{r=r_\mathrm{H}} = \frac{\Omega\, r_\mathrm{H}}{2\pi}\,(B^r)^2\,(\Omega_\mathrm{H} - \Omega)\,\sin^2\theta, \tag{34}$$

where $r_\mathrm{H} = M + \sqrt{M^2 - a^2}$ is the radius of the horizon and $\Omega_\mathrm{H} \equiv a/(2Mr_\mathrm{H})$ can be interpreted as its rotation frequency, which is just the rotation velocity of an Eulerian observer at the apparent horizon. This result implies that if $0 < \Omega < \Omega_\mathrm{H}$ and $B^r \neq 0$, then there is an outward-directed energy flux at the horizon. Therefore, rotational energy is being extracted from the black hole due to the magnetic field lines. The use of Kerr–Schild coordinates allows for direct computations of the flux at the horizon without any special treatment as in Blandford & Znajek (1977) and MacDonald & Thorne (1982). However, one message from this simple calculation is that energy comes out of the event horizon, which is forbidden at the classical level since the horizon is a null surface. The problem lies in the fact that the energy flux defined on other surfaces is not obviously positive definite.

4 NUMERICAL SET-UP

4.1 Diagnostic quantities

To extract physical information, we monitor the rotation frequency of the magnetic field lines (21), which is constant along magnetic field lines on axisymmetric and stationary solutions (Blandford & Znajek 1977), and the Newman–Penrose electromagnetic scalars $\{\Phi_0, \Phi_2\}$, which are computed by contracting the Maxwell tensor with a suitable null tetrad (see e.g. Teukolsky 1973),

$$\Phi_0 \equiv -F^{ab} m_a l_b, \qquad \Phi_2 \equiv F^{ab}\overline{m}_a n_b. \tag{35}$$

The total energy flux (luminosity) of electromagnetic waves, which accounts for the energy carried off by outgoing waves to infinity, is

$$L_\mathrm{EM} = \lim_{r\to\infty} \int r^2 \left(\left|\Phi_2 - \Phi_2^B\right|^2 - \left|\Phi_0 - \Phi_0^B\right|^2\right)\mathrm{d}\Omega, \tag{36}$$

where Φ_2^B and Φ_0^B are the background scalars produced by the steady part of the solution, which vanish only at far distances from the electromagnetic sources. However, since we are considering for simplicity that the magnetic field is produced by a very distant external source, there will be a non-zero contribution to these background scalars induced by the asymptotically uniform magnetic field configuration. An isolated system with no incoming radiation satisfies $\Phi_0 = \Phi_0^B$. Moreover, far from the star the assumption is valid that the background is approximately the same for the incoming and outgoing waves, so that $\Phi_2^B \approx \Phi_0^B$. Combining these relations with the general form given by equation (36), we obtained the simplified formula

$$L_\mathrm{EM} = \lim_{r\to\infty} \int r^2 |\Phi_2 - \Phi_0|^2\,\mathrm{d}\Omega, \tag{37}$$

which has been used previously in several works, reproducing successfully the expected analytical relations (Palenzuela et al. 2009, 2010a; Neilsen et al. 2011). Note that these expressions are equivalent to the radiated energy (30) evaluated at spatial infinity.

4.2 Numerical methods

We will use a finite-difference scheme on a regular Cartesian grid to solve numerically the hyperbolic PDE system. To ensure sufficient resolution in an efficient manner, we employ adaptive mesh refinement (AMR) via the HAD computational infrastructure, which provides distributed, Berger–Oliger style AMR (HAD Team 2002; Liebling 2002) with full subcycling in time, together with an improved treatment of artificial boundaries as has been presented by Lehner, Liebling & Reula (2006). For these simulations, the refinement regions are fixed initially and not changed during the evolution (i.e. fixed mesh refinement).

The spatial discretization is performed by using a fourth-order-accurate scheme satisfying the summation-by-parts rule. The time evolution is performed through the method of lines using a third-order-accurate Runge–Kutta integration scheme with a Courant parameter of $\lambda = 0.25$ such that $\Delta t = 0.25\,\Delta x$ holds at each refinement level.

Our numerical domain consists of a cubical region defined by the intervals $x^i \in [32M, 32M]$ with 61 points in the coarsest grid. We employ a fixed mesh refinement configuration with six levels of refinement, each one covering half of the domain of the parent coarser level. The coarsest resolution employed is $\Delta x = 1.07$ while the finest resolution is $\Delta x = 0.017$. The radii of the different stars in these units are described in Table 1. We have adopted maximally dissipative boundary conditions in our simulations, by setting to zero the time derivative of the electrovacuum incoming modes (Palenzuela et al. 2011).

4.3 Initial data

The initial data for the space–time geometry and the fluid variables produced by rotating stars are obtained by solving the Einstein

Table 1. $M_{\rm b}$ denotes the baryonic mass, $M_{\rm ADM}$ is the gravitational mass, J is angular momentum, Ω is the angular velocity of the fluid, $r_{\rm e}$ is the equatorial radius, $r_{\rm c}$ is the circumferential radius in Schwarzschild coordinates, $w_{\rm c}$ is the metric potential and V_0 is a parameter. All the configurations contain an ergosphere. The ratio between polar and equatorial radii, $r_{\rm p}/r_{\rm e}$, is equal to 0.49 for all the configurations. All numerical values are in units with $G = c = 1$.

V_0	$M_{\rm b}$	$M_{\rm ADM}$	J	Ω	$r_{\rm e}$	$r_{\rm c}$	$w_{\rm c}$
−1.00	0.1814	0.1395	0.0177	1.5685	0.1902	0.3553	1.360
−1.05	0.1885	0.1440	0.1891	1.5844	0.1857	0.3576	1.395
−1.10	0.1998	0.1509	0.0209	1.6103	0.1782	0.3610	1.450
−1.15	0.2018	0.1521	0.0212	1.6151	0.1768	0.3616	1.460
−1.20	0.2080	0.1576	0.0223	1.6298	0.1725	0.3661	1.490

and the hydrodynamic equations with the assumptions of stationarity and axisymmetry. The rotating star solutions have been constructed using the code developed by Ansorg et al. (2002) based on a multidomain spectral method for representing the metric functions. The use of a spectral code was necessary to achieve high accuracy in the case of a stiff equation of state (e.g. for constant total mass–energy density; Bonazzola & Schneider 1974). We consider equilibrium solutions for a rigidly rotating star with an equation of state for homogeneous matter with constant total mass–energy density, μ = constant. For the calculation, we use two different line elements to describe the exterior and interior of the star. The Lewis–Papapetrou line element (18) that covers the exterior has the form

$$\mathrm{d}s^2 = -e^{2\nu}\,\mathrm{d}t^2 + W^2\,e^{-2\nu}\,(\omega\,\mathrm{d}t - \mathrm{d}\phi)^2 + e^{2\alpha}\,(\mathrm{d}\rho^2 + \mathrm{d}\xi^2). \tag{38}$$

The advantage of this line element is that it allows the metric potential ν to remain real inside the ergosphere. For the interior of the star, in the comoving frame of the coordinate, the metric can be expressed as

$$\mathrm{d}s^2 = -e^{2U}\mathrm{d}t^2 + e^{-2U}\left[e^{2k}\,(\mathrm{d}\rho^2 + \mathrm{d}\xi^2) + (W^2 + \eta)\,\mathrm{d}\phi^2\right]. \tag{39}$$

The potential U can be expressed in terms of the lapse function α, while η is the so-called gravitomagnetic potential associated with the shift vector (see Meinel et al. 2008 for a detailed description). Given the particular equation of state and using the conservation of the energy–momentum tensor for the fluid, we obtain inside the star

$$e^{U}\exp\left[\int_0^p \frac{\mathrm{d}p}{\mu + p}\right] = e^{V_0} = \text{constant}. \tag{40}$$

Isobaric surfaces inside the star correspond to a constant value of V_0. At the surface, where pressure goes to zero, it is possible to compute the redshift of a photon emitted with zero angular momentum via

$$z = e^{-V_0} - 1. \tag{41}$$

By changing the parameter V_0, the solution becomes more compact and may contain an ergosphere. We have constructed several rotating stars, with different values of V_0 and rotation frequency Ω. We kept the ratio between the polar and equatorial radii constant. For all the models, the value of the dimensionless spin parameter is roughly constant, $a = J/M^2 \approx 0.9$. The mass, radius and other parameters of the solutions are given in Table 1, where all the solutions listed in the table contain an ergosphere. Our most compact star is close to the limit of maximum compactness $M/R < 4/9 \approx 0.44$ for this family of solutions.

Stationary and asymptotically flat configurations with an ergosphere but without a horizon have been proved to be unstable or marginally unstable under scalar and electromagnetic perturbations (Friedman 1978). For slowly rotating relativistic stars, the time-scale of the instability is shown to be longer than the Hubble time (see e.g. Comins & Schutz 1978). It has been shown by Cardoso et al. (2008) that, for the extreme case of compactness $M/R > 0.5$ and angular momentum $J > 0.4M^2$, the instability time-scales reach 0.1 s for an object with mass of $1M$. In our simulations, however, both the space–time and the fluid are stationary and therefore this instability cannot be active.

The initial data for the black hole are analytical. In the case of spinning black holes, we will use the Kerr–Schild coordinates (Kerr 1963; see e.g. Kramer & Herlt 1980 for more details),

$$g_{ab} = \eta_{ab} + 2Hl_a\,l_b, \tag{42}$$

where η_{ab} is the Minkowsky metric and the scalar function H and the null vector l^b are defined, respectively, by

$$H = \frac{rM}{r^2 + a^2z^2/r^2}, \tag{43}$$

$$l_b = \left(1, \frac{rx + ay}{r^2 + a^2}, \frac{ry - ax}{r^2 + a^2}, \frac{z}{r}\right). \tag{44}$$

The compact object, either a neutron star or a black hole, is immersed in the external magnetic field produced by a distant current loop. This magnetic field is nearly constant initially near the compact object. In addition, it is chosen to be aligned with the spin of the compact object, which is initially oriented along the z-axis. Therefore, the EM fields are initially set to $B^i = B_{\rm o}\,\hat{z}$ and $E^i = 0$ throughout the domain. The field strength $B_{\rm o}$ is irrelevant, since we are assuming that the force-free fields behave like test fields (i.e. they do not modify the curvature of the space–time), and it has been set to $B_{\rm o} = 0.01$. Since we are not considering any coupling between the fluid and the force-free EM fields, the dynamics of the latter will be only influenced by the regular space–time both *inside and outside* the star. For all the effects, there will be no direct interaction between the EM fields and the fluid.

5 RESULTS

In this section, we will describe the dynamics of the force-free fields evolving in the stationary space–times produced by very compact rotating objects with dimensionless spin parameter $a \approx 0.9$. We will concentrate on the cases with the presence of an ergosphere in the space–time (see Appendix A for a discussion on the cases without an ergosphere). We will also analyse the EM power (if any) emitted by the BZ process in these space–times, as well as features of the EM fields after they have relaxed to the stationary solution.

All our simulations display an initial transient, in which the magnetic field is dragged and twisted around the spinning space–time and induces a poloidal electric field. At late times, the EM field relaxes to a stationary state, which is displayed in Fig. 1 for a representative case of a regular space–time with an ergosphere. This case corresponds to $V_0 = -1.20$ (see Table 1). For comparison, we have additionally included the results for the black hole case, a space–time with an ergosphere but also with a horizon which hides a singularity. Further information on the structure of the solutions can be inferred from the currents and charge density of these two cases, as shown in Fig. 2.

In the case of regular space–times with an ergosphere, the magnetic flux near the star is initially expelled, presenting large damped

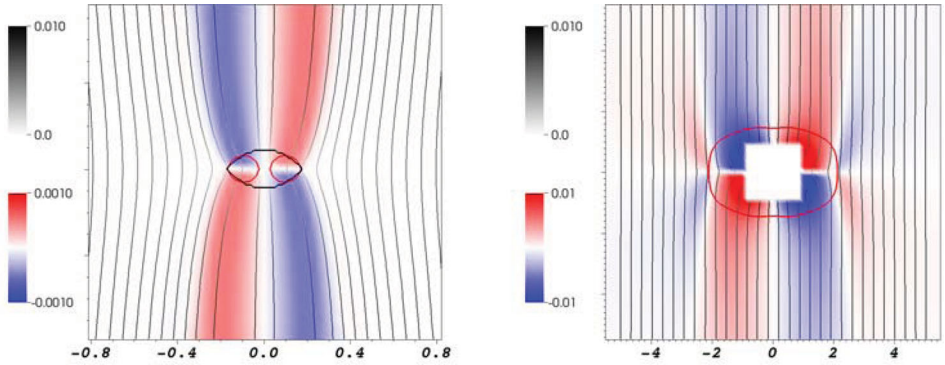

Figure 1. Rotating star and black hole. Magnetic field line components in the plane $x = 0$ after the quasi-stationary state is reached, corresponding to the space–time with an ergosphere (left-hand panel) and to the black hole (right-hand panel). The vertical lines indicate the poloidal component, while the blue–red colours indicate the strength of the component normal to the plane. The structures of these two components of the magnetic field for both cases, star and black hole, are quite similar to each other. The surface of the star is plotted as a black ellipsoid, while the ergosphere is plotted in red.

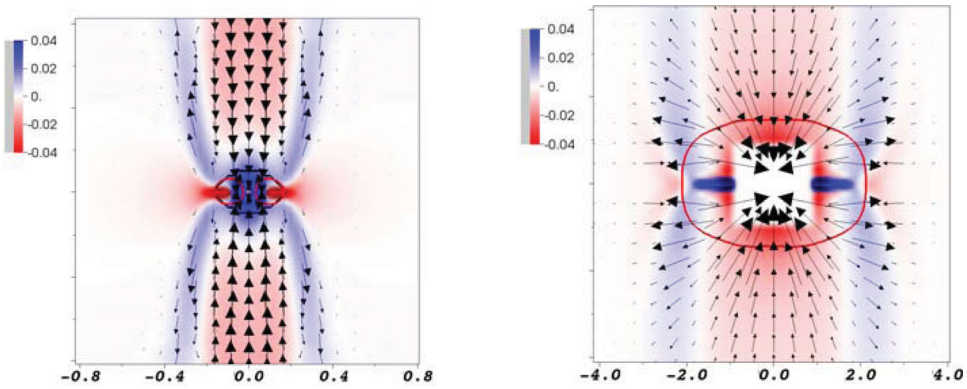

Figure 2. Rotating stars and black hole. Induced charge density (in red–blue colours) and the poloidal currents (in vectors) on the plane $x = 0$ at the quasi-stationary state, corresponding to the same cases as in Fig. 1. The surface of the star is plotted in black and the ergosphere is shown in red lines.

oscillations that relax after a very short time-scale. During this relaxation, which seems to be more relevant as the compactness of the star increases, there is an important isotropic emission of energy. When the stationary state is reached, all the magnetic fields from the region occupied by the star are twisted in the same direction as its angular momentum (in the $z > 0$ domain). The currents in this case are composed of an outflow external cylinder and an inflow inner one. There is also a current sheet where $B^2 \lesssim E^2$ in the intersection of the ergosphere with the equatorial plane, similar to the one that appears in the black hole case (Komissarov 2004; Palenzuela et al. 2010a).

The black hole simulation, on the other hand, relaxes to the stationary state in a shorter time-scale than the above case. The final state resembles the solution corresponding to the regular space–time with an ergosphere, displaying an analogous structure of magnetic fields, currents and charge densities. This clearly indicates that the BZ mechanism acting on the space–times with an ergosphere is basically the same as in the black hole case.

The poloidal structure of the magnetic fields is almost identical in all the simulations, showing that the magnetic flux threading the space–time occupied by the compact object is basically the same. The luminosity, evaluated in a sphere located at $R \approx 10\, r_{\rm e}$ for the stars, and conveniently rescaled for the black hole, is displayed in the left-hand panel of Fig. 3 for all the simulations. The luminosity increases very fast as the compactness of the star increases, although it does not reach the high values of the black hole case.

This smoothness is also found in the angular velocity of the magnetic field, shown in the right-hand panel of Fig. 3, where Ω has been normalized with respect to the central maximum value $\omega_{\rm c}$ for the stars, and with respect to $\Omega_{\rm H}$ for the black hole. As mentioned before, the angular velocity Ω is confined to a small cylinder, showing that the jet is collimated to the region occupied by the compact object. The fast growth of the maximum of this quantity as a function of the compactness of the star can be fitted accurately in this regime to an exponential function, as shown in the left-hand panel of Fig. 4. The luminosity for the different cases can also be represented as a function of the compactness, showing roughly also an exponential dependence in the right-hand panel of Fig. 4.

From our numerical results, we have found the following scaling relations for the angular velocity Ω,

$$\Omega/\omega_{\rm c} \approx A\, {\rm e}^{\lambda\, M/R}, \tag{45}$$

and for the ratio of poloidal and toroidal components of the magnetic field

$$B^{\phi} \approx -f\, \Omega B^{r}, \tag{46}$$

with $f \approx 1/5$ for the space–time with an ergosphere. Note that these estimates contain large sources of error, since they both neglect the details of the space–time geometry and the azimuthal dependence of these quantities. Nevertheless, they can be used to study the behaviour of the solution in different limits and to obtain the correct order of magnitude of the luminosity. By using the line element of our initial data (equation 38), the energy flux density (equation 31)

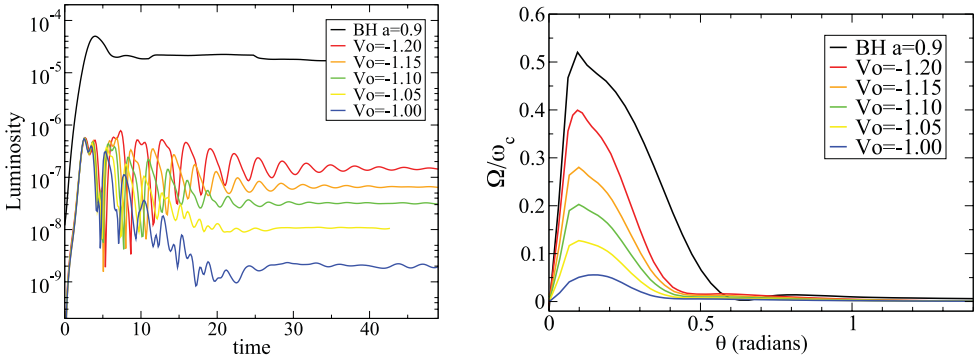

Figure 3. Left panel: the EM luminosity obtained in the rotating space–times with $a = J/M^2 \approx 0.9$. The luminosity increases monotonically with the compactness. Right panel: the angular velocity of the magnetic field Ω, computed at $r \approx 5r_e$ and normalized with respect to its maximum value inside the star (see Table 1).

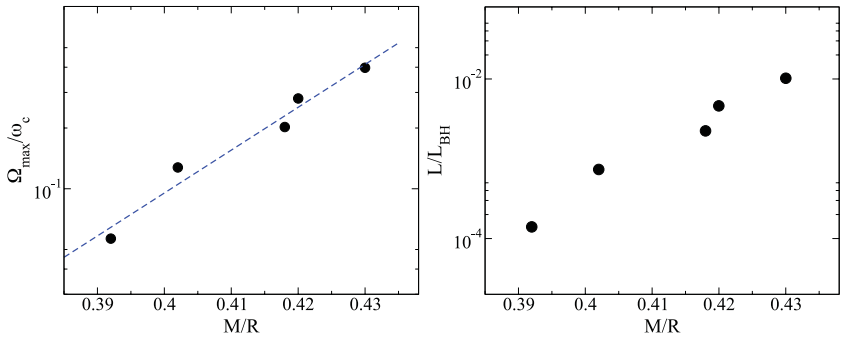

Figure 4. Left panel: the maximum of the (normalized) angular velocity of the magnetic field Ω/ω_c, as a function of the compactness. A fit with the numerical results shows an exponential dependence $A\,e^{\lambda\,M/R}$ with $A \approx 3 \times 10^{-10}$ and $\lambda \approx 50$. Right panel: the EM luminosity calculated in the regular space–times, normalized with respect to the black hole one. Roughly, it also seems to depend exponentially on the compactness.

reduces to

$$S^r_\xi = -\frac{\Omega}{2\pi}\,B^r B^\phi\,W^2 \approx \frac{f\Omega^2}{2\pi}\,(B^r)^2 W^2 \approx \frac{A f \omega_c^2}{2\pi}\,(B^r)^2\,W^2\,e^{2\lambda\,M/R}, \tag{47}$$

which is a positive definite quantity, and where we have used subsequently the above approximations. Note that the scaling is similar to the BZ power in equation (34), except by the exponential dependence on the compactness, and is consistent with the results shown in the right-hand panel of Fig. 4.

6 CONCLUDING REMARKS

We have studied the evolution of EM fields on rotating and highly compact regular space–times with an ergosphere. Our results show that if an ergosphere is present, the structure of EM fields and currents is similar to the black hole ones. This implies that the same mechanism operates in both space–times, independent of the presence/absence of a horizon. Note that these results are in agreement with the fact that the BZ process is not an effect caused by the horizon, as was pointed out by Komissarov (2004, 2005) in the context of black holes.

In the case of a realistic rotating star, the fluid will be coupled with the EM fields and, therefore, they are forced to rotate following the fluid. So, the extraction process can be described by the simple model of the Faraday disc, which is even more efficient than the BZ process. In this case, the twist on the magnetic field will be dominated not by the space–time but by the fluid rotation. In general, the strong dependence of Ω on the compactness will imply a low-energy extraction on regular space–times even if matter is not present.

An example of regular and rotating space–time may be produced by an orbiting binary black hole system, as considered by Lyutikov (2011). In this work, it was suggested that the rotation of the space–time inside the binary system, induced by the orbital motion of the black holes, would allow for two different channels of energy extraction: through the generalized BZ in boosted (and maybe rotating) black holes, which will produce a dual jet structure (Palenzuela et al. 2010b), and through the BZ process on regular space–times inside the binary system. However, the lack of an ergosphere in the central region will probably prevent the activation of the BZ process (see Appendix A for a discussion on the case of space–times without ergosphere). Even if the BZ process takes place, and assuming that the luminosity still follows the exponential dependence shown earlier, the low compactness of the space–time in this central region will induce a faint jet that will be overshined by the BZ process taping kinetic energy (either translational or rotational) directly from the black holes.

Summarizing, we have found that the BZ process is also present on regular space–times with an ergosphere. Our conclusive results imply that we have to reconsider the membrane paradigm as a tool to explain the BZ mechanism, which also seems to be able to extract energy from rotating regular space–times with ergospheres and boosted non-rotating black holes.

ACKNOWLEDGMENTS

We are in debt to L. Lehner and T. Garrett for stimulating discussions about the origin of the BZ process which initiated this project. We

are also grateful to Marcus Ansorg and his collaborators for giving us access to his spectral code, and for the useful discussions on spectral method during his period at AEI. It is a pleasure to thank L. Lehner, S. Liebling, S. Komissarov and C. Thompson, as well as our long-term collaborators M. Anderson, E. Hirschmann and D. Neilsen, for useful discussions and comments on this paper.

We acknowledge support from the Spanish Ministry of Science and Innovation under grants CSD2007-00042, CSD2009-00064 and FPA2010-16495, and Govern de les Illes Balears. Computations were performed in Scinet and Mare Nostrum (funded by BSC grant FI-2011-3-0017).

REFERENCES

Ansorg M., Kleinwachter A., Meinel R., 2002, A&A, 381, L49
Bergamini R., Viaggiu S., 2004, Class. Quantum Gravity, 21, 4567
Blandford R. D., Znajek R. L., 1977, MNRAS, 179, 433
Bonazzola S., Schneider S., 1974, ApJ, 191, 273
Cardoso V., Pani P., Cadoni M., Cavaglia M., 2008, Phys. Rev. D, 77, 124044
Comins N., Schutz B., 1978, Proc. R. Soc. London A, 364, 211
Friedman J. L., 1978, Commun. Math. Phys., 63, 243
Goldreich P., Julian W. H., 1969, ApJ, 157, 869
Gruzinov A., 2007, preprint (arXiv:0710.1875)
HAD Team, 2002, The HAD code = , http://relativity.phys.lsu.edu/~matt/had.html
Kerr R. P., 1963, Phys. Rev. Lett., 11, 237
Komissarov S. S., 2002, arXiv:astro-ph/0211141
Komissarov S. S., 2004, MNRAS, 350, 407
Komissarov S. S., 2005, MNRAS, 359, 801
Komissarov S. S., 2009, J. Korean Phys. Soc., 54, 2503
Kramer D., Stephani H., Herlt E., MacCallum M., 1980, Exact Solutions of Einstein's Field Equations. Cambridge Univ. Press, Cambridge
Lehner L., Liebling S. L., Reula O., 2006, Class. Quantum Gravity, 23, S421
Lewis T., 1932, Proc. R. Soc. London A, 136, 176
Liebling S. L., 2002, Phys. Rev. D, 66, 041703
Lyutikov M., 2011, Phys. Rev. D, 83, 064001
MacDonald D., Thorne K. S., 1982, MNRAS, 198, 345
McKinney J. C., Gammie C. F., 2004, ApJ, 611, 977
Meinel R., Ansorg M., Kleinwächter A., Neugebauer G., Petroff D., eds, 2008, Relativistic Figures of Equilibrium. Cambridge Univ. Press, Cambridge
Neilsen D., Lehner L., Palenzuela C., Hirschmann E. W., Liebling S. L., Motl P. M., Garrett T., 2011, Proc. Natl Acad. Sci., 108, 12641
Palenzuela C., Anderson M., Lehner L., Liebling S. L., Neilsen D., 2009, Phys. Rev. Lett., 103, 081101
Palenzuela C., Bona C., Lehner L., Reula O., 2011, Class. Quantum Gravity, 28, 134007
Palenzuela C., Garrett T., Lehner L., Liebling S. L., 2010a, Phys. Rev. D, 82, 044045
Palenzuela C., Lehner L., Liebling S. L., 2010b, Sci, 329, 927
Papapetrou A., 1966, Ann. Inst. Henri Poincaré A, 4, 83
Punsly B., Coroniti F. V., 1989, Phys. Rev. D, 40, 3834
Punsly B., Coroniti F. V., 1990, ApJ, 350, 518
Spitkovsky A., 2006, ApJ, 648, L51
Tchekhovskoy A., Narayan R., McKinney J. C., 2010, ApJ, 711, 50
Teukolsky S. A., 1973, ApJ, 185, 635
Thorne K. S., Macdonald D., 1982, MNRAS, 198, 339
Thorne K. S., Price R. H., Macdonald D. A., 1986, The Membrane Paradigm. Yale Univ. Press, New Haven, CT

APPENDIX A: ROBUSTNESS OF THE RESULTS

We have checked the robustness of our solutions against several sources of error. One of the possible problems may come from the way in which the analysis quantities are evaluated. In particular, the surface where the luminosity is computed may be located too close to the source, where the space–time is still far from being flat, producing an error in that measure. We have compared the luminosity computed in two surfaces located at $5\,r_e$ and $10\,r_e$ for the case with $V_0 = -1.2$, obtaining a difference smaller than 5 per cent. Another potential problem may come from the influence of the boundary conditions, which may produce unphysical reflections which may affect, after a light-crossing time, the dynamics of the system. In our simulations, this is not a problem since the solution relaxes to the stationary state before a light-crossing time, and it remains unaffected afterwards.

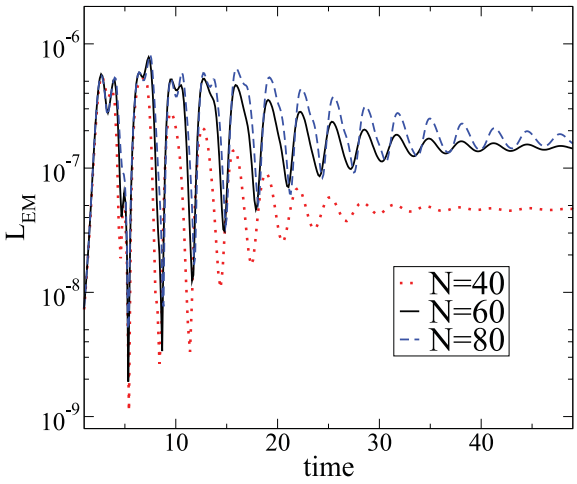

Figure A1. EM luminosity for the case $V_0 = -1.2$ (with an ergosphere) for three different spatial numerical resolutions with $N = \{40, 60, 80\}$ points in the coarsest grid. The luminosity converges with the expected fourth-order convergence.

Probably the most important source of inaccuracies comes from numerical discretization errors. We have compared three different spatial resolutions, corresponding to $N = \{40, 60, 80\}$ points in the coarsest grid. Our comparisons are summarized in Fig. A1, where we have restricted our analysis to a representative case corresponding to $V_0 = -1.2$. Note that in this case, there is an ergosphere, and consequently a current sheet on the equatorial plane which is difficult to represent on a discretized grid. Nevertheless, the luminosity displays the expected fourth-order convergence to a well-defined solution.

We have also tried to study the relaxed solutions of space–times without an ergosphere. Although the luminosity reaches a quasi-stationary value, it changes dramatically with resolution and does not seem to converge to a unique solution. This lack of convergence is shown in the left-hand panel of Fig. A2 for a representative case without an ergosphere corresponding to $V_0 = -0.97$. In these cases, there is a violation of the force-free condition, as can be seen in the right-hand panel of Fig. A2. The poloidal currents inside the star are not parallel to the poloidal magnetic field, a consequence of a non-vanishing toroidal electric field. This component has to vanish in stationary and axisymmetric space–times. Our guess is that there is no force-free solution with these boundary conditions unless a current sheet appears, and so the numerical evolution relaxes only to an approximated solution which depends strongly on the resolution. More work is needed to elucidate this issue, maybe considering the full MHD problem instead of the force-free limit.

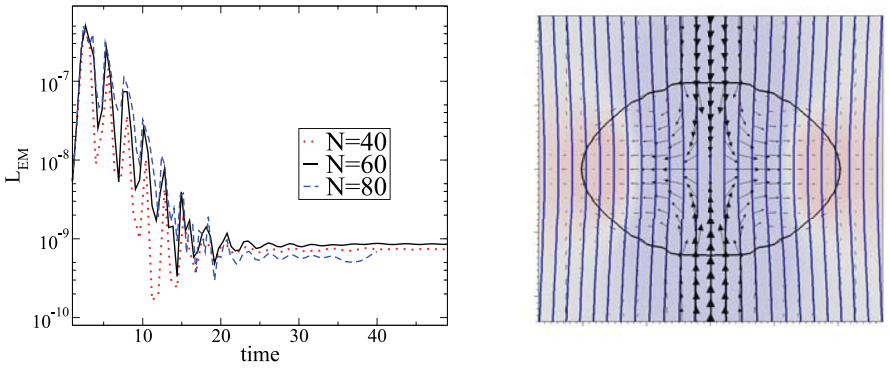

Figure A2. Left panel: EM luminosity for the same three different resolutions as in Fig. A1. In this case, the solutions do not display any convergence. Right panel: poloidal magnetic field lines (in blue) and poloidal current vectors (in black) in the $x = 0$ plane after the quasi-stationary state is reached, corresponding to the space–time without an ergosphere. The blue–red colours indicate the charge density, while the black ellipsoid represents the surface of the star. Although the poloidal component of these fields has to be parallel in a force-free stationary and axisymmetric solution, it is clearly not satisfied in the interior of the star.

This paper has been typeset from a TEX/LATEX file prepared by the author.